

Tutorial on the Impact of Network Parameters on Distance Element Resistance Coverage

Gabriel Benmouyal, Armando Guzmán, and Rishabh Jain
Schweitzer Engineering Laboratories, Inc.

Presented at the
40th Annual Western Protective Relay Conference
Spokane, Washington
October 15–17, 2013

Tutorial on the Impact of Network Parameters on Distance Element Resistance Coverage

Gabriel Benmouyal, Armando Guzmán, and Rishabh Jain, *Schweitzer Engineering Laboratories, Inc.*

Abstract—Mho elements used for the protection of transmission lines have a distance reach setting but do not have a resistance reach setting. Quadrilateral elements offer both distance and resistance reach settings. The resistance coverage or how much fault resistance a mho element will be able to detect depends on the natural response of the element. For quadrilateral elements, the resistance coverage depends upon the resistance reach setting but is not necessarily always equal to this latter value. The purpose of this paper is to identify factors that determine the resistance coverage for both the mho and quadrilateral elements. These factors are the network parameters such as the source and transmission line sequence impedances, the distance to the fault, and, in the case of quadrilateral elements, the resistance reach setting. Some basic rules are derived based on the testing of elementary networks.

I. INTRODUCTION

Mho elements for the protection of transmission lines do not have a reputation for extensive resistance coverage. In this paper, the resistance coverage for a distance element (mho or quadrilateral) means the maximum fault resistance that the element is able to detect at a given distance from the relay on the transmission line. Quadrilateral elements have been devised to overcome this shortcoming and are considered to have greater resistance coverage than mho elements do. In order to achieve this greater coverage, quadrilateral distance elements have an additional setting: the resistance reach or resistance setting. Contrary to what might be initially assumed, the resistance setting does not behave like the distance setting: whereas the distance setting constitutes, in most cases, the maximum distance at which the element will detect a fault, the resistance setting does not necessarily constitute the maximum fault resistance that the element can detect.

When implementing changes on elementary networks such as a single transmission line between two sources, we rapidly realize that the resistance coverage of both mho and quadrilateral elements does not remain constant and will vary with the distance to the fault, line loading, and changes occurring in the sources and transmission line impedances. These last three items identify the network parameters that are varied in the study described in this paper in order to evaluate the change in the resistance coverage. Changes in the resistance coverage of distance elements will also occur if changes are implemented in the network configuration, such as the addition of a parallel line with or without mutual coupling.

Besides the evaluation of the impact of changing network parameters on the resistance coverage of distance elements,

the other objective of this paper is to establish an analytical relation between the network parameters of an elementary network and the maximum fault resistance $R_{f,max}$ that a fault detector (mho or quadrilateral) can detect.

In this paper, we concentrate on single-phase-to-ground fault detectors.

II. THE GENERIC EQUATION OF IMPEDANCE RELAYING

A. Elementary Network With a Single Transmission Line

Consider the elementary power network in Fig. 1, consisting of a single transmission line supplied by two ideal voltage sources. Equation (1) is the generic equation on which impedance relaying is based. This equation is applicable to a distance or impedance element located at the left bus and looking toward the right or remote source.

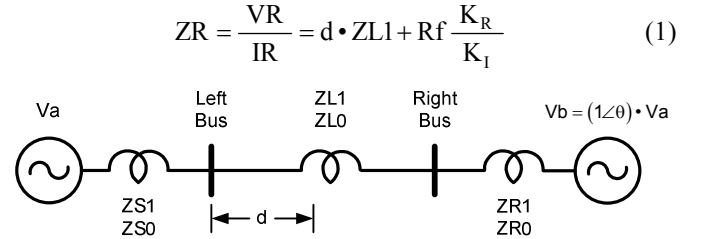


Fig. 1. Elementary power system

The demonstration of (1) is provided in Appendix A, where all its variables are identified for the case of Phase A-to-ground faults. For any impedance loop considered and shown in Table I, (1) is the expression of the apparent impedance seen by the distance (ANSI 21) element when supplied with the proper voltage V_R and current I_R required by the particular impedance loop. The first term to the right of the equal sign (i.e., $d \cdot Z_{L1}$) is the term that protection engineers are most familiar with. It expresses the property that the apparent impedance is proportional to the positive-sequence (PS) impedance of the line Z_{L1} , the constant of proportionality being the distance to the fault d . The second term (i.e., $R_f \cdot K_R/K_I$) is proportional to the fault resistance R_f and is considered to be an added error that is most of the time ignored by protection engineers. However, it is typically taken into account in studies dealing with fault location [1]. Mho characteristic distance protection is based on the assumption that the fault resistance will be small, and this assumption has been justified by decades of successful practice and verification. When significant fault resistance is expected, mho elements are conventionally supplemented with distance quadrilateral elements, providing better fault resistance coverage.

TABLE I
IMPEDANCE LOOP VOLTAGES AND CURRENTS

Fault Type	VR	IR	K_R
A-G	VA	IA + K0 • I0	$K_R = \frac{3}{[2C1 + C0(1 + K0)]}$
B-G	VB	IB + K0 • I0	$K_R = \frac{3}{[2C1 + C0(1 + K0)]}$
C-G	VC	IC + K0 • I0	$K_R = \frac{3}{[2C1 + C0(1 + K0)]}$
A-B, A-B-G	VA - VB	IA - IB	$K_R = \frac{1}{2 \cdot C1}$
B-C, B-C-G	VB - VC	IB - IC	$K_R = \frac{1}{2 \cdot C1}$
C-A, C-A-G	VC - VA	IC - IA	$K_R = \frac{1}{2 \cdot C1}$
A-B-C, A-B-C-G	V1	I1	$K_R = \frac{1}{C1}$

Table I provides the expressions of VR and IR for the six possible impedance loops: three ground faults and three phase faults. In Table I, we have added a seventh impedance loop that is three-phase fault detection based on the use of the positive-sequence voltage (PSV) and current. In reality, this seventh loop is not used because three-phase faults will be detected by the three phase-based impedance loops. In Table I, the current I0 is the zero-sequence (ZS) current at the relay location, whereas K0 is the ZS compensating factor defined by (50) in Appendix A. The same derivation principles applied in Appendix A for Phase A-to-ground faults can be applied to the other impedance loops shown in Table I.

Table II provides the exact location and identification of the fault resistance for the different impedance loops.

The term K_R is a function of the PS and ZS current distribution factors and is provided in Table I for each impedance loop. The expressions of the PS and ZS current distribution factors (or ratio of the sequence current at the relay location over the same sequence current at the fault location) as a function of the distance d to the fault and the network impedances are:

$$C1 = C2 = \frac{I1}{I1F} = \frac{I2}{I2F} = \frac{ZR1 + (1-d)ZL1}{ZL1 + ZS1 + ZR1} \quad (2)$$

$$C0 = \frac{I0}{I0F} = \frac{ZR0 + (1-d)ZL0}{ZL0 + ZS0 + ZR0} \quad (3)$$

TABLE II
FAULT RESISTANCE LOCATION

Fault Type	Fault Resistance Location
A-G (shown) B-G C-G	
A-B B-C (shown) C-A	
A-B-G B-C-G (shown) C-A-G	
A-B-C	

The term K_I is equal to the ratio of the fault current, represented by IR , for a particular impedance loop over the difference between the current IR and its value prior to the fault (i.e., the load current). For systems operated with no load current prior to the fault, the term K_I is simply equal to 1.

$$K_I = \frac{IR}{IR - IR_{\text{prefault}}} = \frac{IR}{\Delta IR} \quad (4)$$

Equation (1) allows us to relate the fault resistance to the particular impedance loop voltage and current. It also allows us to extract the value of the fault resistance once the fault type is identified.

$$Rf = \left(\frac{VR}{IR} - d \cdot ZL1 \right) \cdot \frac{K_I}{K_R} \quad (5)$$

Equation (5) underscores the virtual impossibility of calculating the fault resistance using the transmission line single-ended data. We would need to know the exact fault location and the two source impedances in order to be able to calculate K_R . The load current prior to the fault also needs to be known. This explains the approximations in the conventional resistance blinder calculations as found in quadrilateral elements and described later in this paper.

B. Elementary Network With Parallel Lines Without Mutual Coupling

Consider the power circuit of Fig. 2. This is simply the elementary network of Fig. 1 to which a parallel transmission line without mutual coupling has been added.

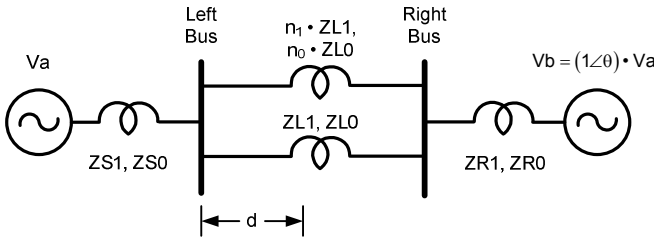


Fig. 2. Elementary network with parallel lines

Does (1) still apply for distance elements implemented on the left terminal of the bottom line? The answer is yes for the impedance loop voltages and currents as provided by Table I, but the factor K_R has to be changed to the following:

$$K_R = \frac{3}{[2C1_p + C0_p(1 + K0)]} \quad (6)$$

In (6), the current distribution factors are no longer provided by (2) and (3) but are now equal to the following (see Appendix A):

$$C1_p = C2_p = \frac{(1 + n_1 - d) \cdot ZR1 + (1 - d) \cdot ZS1 + (1 - d) \cdot n_1 \cdot ZL1}{(1 + n_1) \cdot (ZS1 + ZR1) + n_1 \cdot ZL1} \quad (7)$$

$$C0_p = \frac{(1 + n_0 - d) \cdot ZR0 + (1 - d) \cdot ZS0 + (1 - d) \cdot n_0 \cdot ZL0}{(1 + n_0) \cdot (ZS0 + ZR0) + n_0 \cdot ZL0} \quad (8)$$

Equations (7) and (8) are used later in this paper when establishing the relation between element resistance coverage and the network parameters.

III. THE RESISTANCE COVERAGE OF MHO ELEMENTS

A. The Implementation of Mho Elements

Implementing a conventional impedance or distance (ANSI 21) element with a mho characteristic is done by defining one operating vector and one polarizing vector as in the following:

$$\begin{aligned} S_{\text{op}} &= D \cdot ZL1 \cdot IR - VR \\ S_{\text{pol}} &= V_{\text{pol}} \end{aligned} \quad (9)$$

In (9), D is the element distance reach in per unit of the line length, $ZL1$ is the line positive-sequence impedance, IR is the current supplied at the input of the element, and VR is the voltage at the input of the element.

Conventional voltage polarizing quantities (V_{pol}) include self-polarization, cross-polarization, polarization by positive-sequence phasor voltage ($V1$), and, finally, polarization by positive-sequence voltage memory ($V1M$).

The element asserts when the scalar product between the operating quantity and the polarizing quantity is positive or when it satisfies (10).

$$\text{real}[(D \cdot ZL1 \cdot IR - VR) \cdot V_{\text{pol}}^*] \geq 0 \quad (10)$$

In (10), *real* represents *real part of* and the asterisk points to the *complex conjugate of*. The scalar product is tantamount to implementing an angle comparator: if the angle between the polarizing quantity and the operating quantity is less than 90 degrees, the element asserts.

An alternate solution to the scalar product of (10) is to calculate the distance quantity m as follows [2]:

$$m = \frac{\text{real}[VR \cdot V_{\text{pol}}^*]}{\text{real}[ZL1 \cdot IR \cdot V_{\text{pol}}^*]} \quad (11)$$

Provided the denominator in (11) is positive, the next step is to verify that the calculated distance m is smaller than the set reach in order to assert the element.

$$m \leq D \quad (12)$$

In order to cover all possible fault types on a transmission line, the relay has to process six impedance loops, three for ground faults and three for phase faults. Each impedance loop requires a particular voltage VR and current IR . The expressions of VR and IR for the six possible loops are provided in Table I.

B. Analytical Relation Between Ground Mho Element Resistance Coverage and the Network Parameters

For the elementary power system in Fig. 1 for which the generic equation of impedance relaying has been derived, it would be practical to obtain a mathematical expression for the resistance coverage as a function of the network parameters.

Based on the generic equation, the operating and polarizing quantities for the Phase A-to-ground mho element are provided as:

$$\begin{aligned} S_{op} &= D \cdot ZL1 \cdot (IA + K0 \cdot I0) - VA \\ S_{pol} &= V_{pol} \end{aligned} \quad (13)$$

From (1), the current at the relay can be expressed as:

$$(IA + K0 \cdot I0) = \frac{VA}{d \cdot ZL1 + Rf \cdot \frac{K_R}{K_I}} \quad (14)$$

Introducing (14) into the operating quantity in (13), we obtain:

$$S_{op} = \left[\frac{D \cdot ZL1}{d \cdot ZL1 + Rf \cdot \frac{K_R}{K_I}} - 1 \right] \cdot VA \quad (15)$$

The element will assert when the scalar product between the operating and polarizing quantities is greater than or equal to zero, or:

$$\text{real} \left[\left[\frac{D \cdot ZL1}{d \cdot ZL1 + Rf \cdot \frac{K_R}{K_I}} - 1 \right] \cdot VA \cdot V_{pol}^* \right] \geq 0 \quad (16)$$

Assuming self-polarization, we have:

$$VA \cdot V_{pol}^* = VA \cdot VA^* = |VA|^2 \quad (17)$$

We shall see later in this paper that the mho element resistance coverage is somehow affected by the load current. If we assume zero load, the factor K_I in (16) can be set to 1. Equation (16) simply becomes:

$$\text{real} \left[\frac{D \cdot ZL1}{d \cdot ZL1 + Rf \cdot K_R} - 1 \right] \geq 0 \quad (18)$$

In (18), replacing K_R by its expression in Table I, the equation for the maximum resistance coverage is obtained by using the equal sign:

$$\text{real} \left[\frac{D \cdot ZL1}{d \cdot ZL1 + \frac{3 \cdot Rf_{max}}{[2 \cdot C1 + C0 \cdot (1 + K0)]}} - 1 \right] = 0 \quad (19)$$

Equation (19) allows the calculation of Rf_{max} as a function of the network parameters only if self-polarization and zero load current are assumed. If we assume another type of polarization such as polarization by PSV, we end with:

$$\text{real} \left[\left[\frac{D \cdot ZL1}{d \cdot ZL1 + Rf \cdot K_R} - 1 \right] \cdot VA \cdot V1^* \right] \geq 0 \quad (20)$$

In (20), there is no guarantee that the angle between VA and $V1$ is equal in all conditions, so we cannot make the voltages disappear from the equation, as in the case of self-

polarization. Our attempt to derive an expression for the resistance coverage as a function of the network parameters is possible then only for the self-polarization case. Unfortunately, this is the least interesting because it is not used very often.

C. The Resistance Coverage of Ground Mho Elements

When considering a mho element, there is only the distance reach setting D that is introduced in the base equation provided by (13). Because there is no resistance setting, the resistance coverage of a mho element has to be considered as intrinsic to its characteristics.

1) Impact of the Polarizing Voltage

Consider the elementary 230 kV single-line network of Fig. 1 as shown in Fig. 3 with specific sources and transmission line impedances. All resistance values obtained from tests on this network are shown in the rest of this paper in primary values. Assume a single-Phase A-to-ground fault is applied at a distance d from the left bus. We want to investigate the resistance coverage of the mho ground element when three types of polarizing voltages are applied: self-polarization, PSV polarization, and PSV memory. Assuming a distance reach D for the element of 100 percent of the line length, the results are shown in Fig. 4. The line loading angle has been set to 0 degrees.

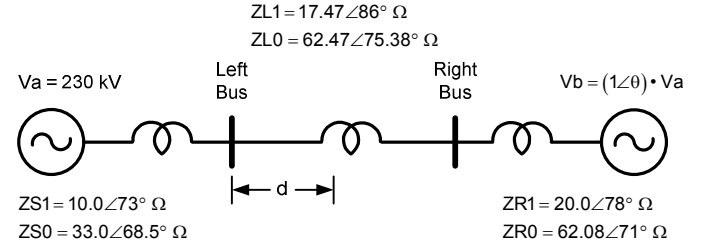


Fig. 3. Single-line power network

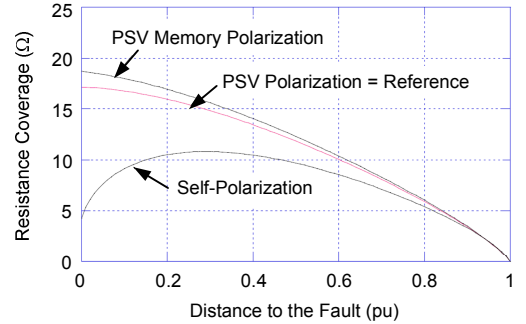


Fig. 4. Impact on resistance coverage of voltage polarization for the mho ground element at zero load

From Fig. 4, it is obvious that the best resistance coverage is obtained with PSV memory polarization. The second-best coverage (very close to the previous) is PSV polarization. Finally, doing very poorly (at least with distance d close to the relay), we have self-polarization.

For the remaining testing, we use PSV polarization, because it has better resistance coverage than the self-polarized mho and is most commonly used in the industry.

2) Network-Based or Equation-Based Approach to Determine $R_{f_{max}}$

When trying to determine the mho ground element resistance coverage as a function of the fault location, there are two possible methods.

The first approach is to solve the network equations as indicated in Appendix A, obtain the voltage and current at the relay for a particular fault resistance value, and introduce these values in (10). Repeat the same process with increasing values of fault resistance until inequality (10) no longer holds. The maximum fault resistance found provides the value of the resistance coverage $R_{f_{max}}$. This process has to be repeated for different values of fault location in order to get a plot of the resistance coverage as a function of the fault location.

The second approach is to solve the equation of $R_{f_{max}}$ as a function of the network parameters when this equation is available.

Because the search for an analytic equation providing the value of $R_{f_{max}}$ as a function of the network parameters in the case of the PSV polarization has been so far unsuccessful, we use the network-based solution in the next subsections.

3) Impact of the Line Loading

For the network of Fig. 3, Fig. 5 shows the resistance coverage for the Phase A ground mho element when the line loading takes the values -10 , 0 , and 10 degrees. Obviously, the line loading has some impact on the resistance coverage.

The fact that the line loading has some effect on the resistance coverage calculation indicates that the factor K_1 in (16) cannot be set simply to 1.

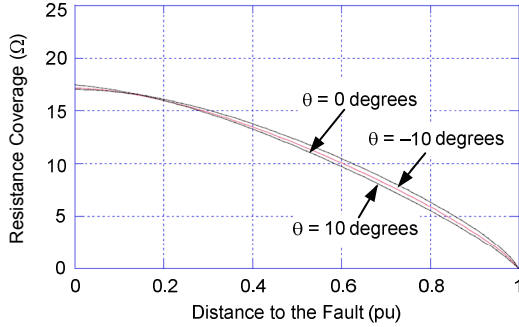


Fig. 5. Impact on resistance coverage of the line loading for the mho ground element

4) Impact of the Set Distance Reach D

If we look at (18), we can see that the mho element distance reach setting D is involved in the solution of the resistance coverage. This indicates that $R_{f_{max}}$ will depend upon the distance setting D . This is illustrated in Fig. 6, where D has been set successively to 0.6, 0.8, and 1. The line loading angle has been set to 0 degrees (no load) for these plots.

Obviously, the maximum fault resistance detected occurs at distance to fault d equal to zero. It is interesting to observe from Fig. 6 that the resistance coverage at the distance reach setting D is always equal to zero.

Fig. 6 allows us to infer that the distance reach setting and the resistance coverage in a mho element are interrelated: setting the distance reach D will determine the resistance coverage characteristic.

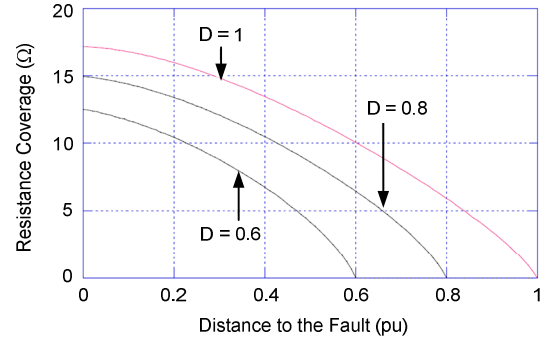


Fig. 6. Impact on resistance coverage of distance reach setting for the mho ground element at zero load

5) Definition of a Reference Network

For the remaining testing of the resistance coverage of the Phase A ground mho element, we define a reference network corresponding to the following:

- The network of Fig. 3 with a loading angle θ of 0 degrees.
- Use of PSV polarization.
- Distance reach D set at 100 percent of line length.

The source-to-line impedance ratio (SIR) of the reference network for the left source is 0.57 and for the right source is 1.14. In this paper, the SIR is defined as the ratio of the source PS impedance divided by the element impedance reach. Both SIRs are considered as having low values or as being strong sources.

In Fig. 7 through Fig. 12, the plot of the resistance coverage for the ground mho element corresponding to the reference network is shown in red.

6) Impact of the Right Source Impedance

In Fig. 7, the impact of the right source impedances is evaluated by setting its PS and ZS impedances at 0.1 and 10 times their original values. A last test is performed with the impedances close to infinity.

Obviously, when compared with the reference network, the effect of reducing the right source sequence impedances is to reduce the resistance coverage. Conversely, increasing the right source sequence impedances leads to greater resistance coverage. The right source sequence impedances getting closer to infinity corresponds to a radial system, and greater resistance coverage is obviously achieved.

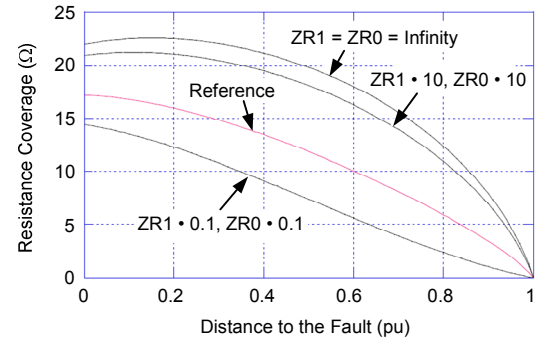


Fig. 7. Impact on resistance coverage of the right source sequence impedances for the mho ground element

7) Impact of the Left Source Impedance

In Fig. 8, the impact of the left source impedances is evaluated by setting its PS and ZS impedances at 0.1 and 10 times their original values.

Increasing the left source sequence impedances has the effect of reducing the resistance coverage.

Decreasing the left source sequence impedances has a mixed effect: the resistance coverage is reduced for small values of the distance to the fault d and it is slightly increased for higher values of the fault distance d .

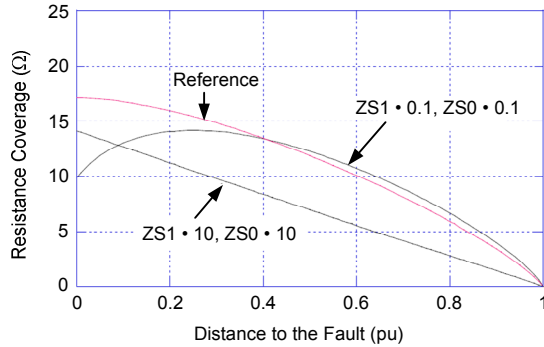


Fig. 8. Impact on resistance coverage of the left source sequence impedances for the mho ground element

An additional test has been performed in Fig. 9 where the right source sequence impedances have been set to infinity and the left source original PS and ZS impedances multiplied by factors of 0.1 and 10.

We can see in Fig. 9 that with no infeed to the fault (radial system), the impact of the source behind the relay sequence impedance variation is practically the inverse of the previous case. There is greater resistance coverage with the increase of the impedance magnitudes and lesser resistance coverage with the decrease of the impedance magnitudes.

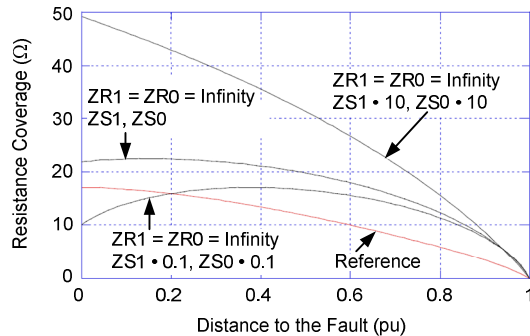


Fig. 9. Impact on resistance coverage of the left source sequence impedances with a radial network for the mho ground element

8) Impact of the Transmission Line Impedance

As shown in Fig. 10, increasing the transmission line sequence impedances by a factor of 10 has the effect of substantially increasing the mho element resistance coverage.

Conversely, decreasing the line sequence impedances by a factor of 10 has the effect of substantially reducing the element resistance coverage.

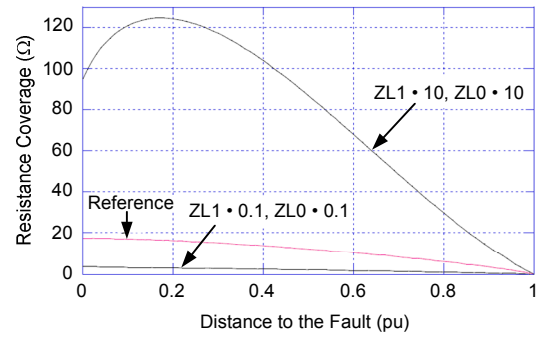


Fig. 10. Impact on resistance coverage of the transmission line sequence impedances for the mho ground element

Based on the testing results in Fig. 7 and Fig. 10, we can infer that a substantial resistance coverage would be achieved with a radial system and a very long line. This is demonstrated in Fig. 11, where the right source impedances have been set to infinity and the line impedances multiplied by 10.

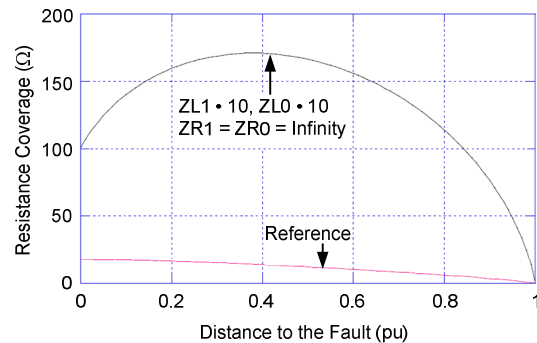


Fig. 11. Mho ground element optimum resistance coverage

9) Impact of the Open Breaker Condition at the End of the Line

The open breaker condition at the end of the line corresponds simply to the simulated case where the remote source has sequence impedances close to infinity.

In Fig. 7, with the breaker closed, the ground mho element resistance coverage corresponds to the red plot noted as the reference. When the breaker opens, the resistance coverage plot corresponds to the plot identified as $ZR1 = ZR0 = \text{Infinity}$.

Obviously, the breaker status at the end of the line leads to two different resistance coverage characteristics.

10) Impact of a Parallel Line

The impact of a parallel line as shown for the network in Fig. 2 can be assessed by looking at Fig. 12, where the factor n multiplying the sequence impedances (from Fig. 2, $n = n_1 = n_0$) of the adjacent line has been set successively to 0.25, 1, and 4.

Obviously as the factor n is increased, the resistance coverage characteristic tends to get closer to the reference network plot in red. Overall, a parallel line cannot be considered to have a significant impact.

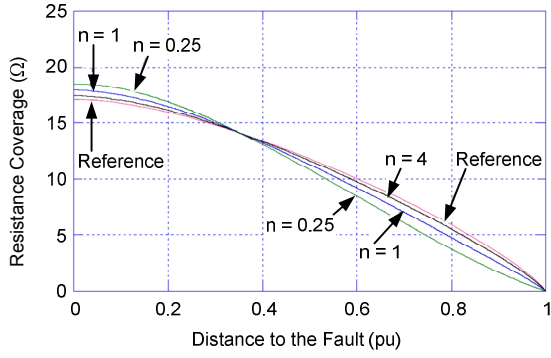


Fig. 12. Impact on resistance coverage of parallel line for the mho ground element

IV. THE RESISTANCE COVERAGE OF QUADRILATERAL ELEMENTS

A. The Implementation of Quadrilateral Characteristics

Quadrilateral distance characteristics can take various forms. Fig. 13 shows a typical characteristic. While the mho element is essentially self-directional and requires the computation of a single scalar product as in (10), the quadrilateral characteristic requires the implementation of a minimum of three independent elements:

- A reactance element that determines the distance reach.
- Two resistance blinders that determine the resistance reach setting.
- One directional element that determines if the fault is forward or reverse.

It is important to note here that the resistance blinder calculation is independent from the other elements. Because it constitutes the focus of this paper, the next subsections concentrate on the resistance calculation only.

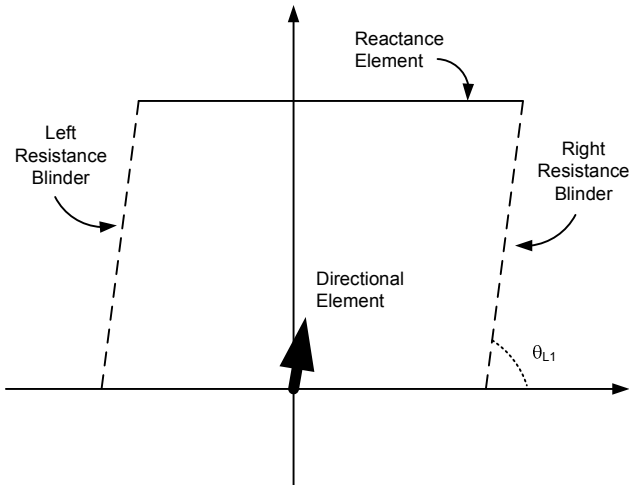


Fig. 13. Quadrilateral characteristic components

B. How to Set the Resistance Reach

There is a limit to the value given to the resistance reach R_{set} of a quadrilateral element. This limit is essentially imposed by the accuracy of the voltage and current transformers supplying the relay with respect to the phase angle. References [3] and [4] introduced formulas for the

calculation of the maximum possible resistance reach value as a function of an error angle that is the sum of all possible phase angle errors. In [4], the maximum resistance reach value for a Zone 1 element is provided by:

$$R_{set,max} = \frac{\sin(\theta_\epsilon + \theta_{L1})}{\sin(\theta_\epsilon)} \cdot (1 - Z_{set,pu}) \cdot |ZL1| \quad (21)$$

In (21), θ_ϵ is the total phase angle error, θ_{L1} is the line PS impedance angle, $Z_{set,pu}$ is the reactance element reach in per-unit value, and finally, $|ZL1|$ is the line PS impedance magnitude.

If we assume a total phase angle error of 2 degrees and a distance reach of 80 percent of the line, we have the following for the maximum possible resistance reach of the quadrilateral elements installed at the ends of the network transmission line:

$$R_{set,max} = \frac{\sin(88^\circ)}{\sin(2^\circ)} \cdot 0.2 \cdot 17.47 = 100.06 \Omega \quad (22)$$

In the remaining testing, we use a resistance reach of 80 ohms.

C. First Example of Resistance Blinder Calculation

Our first example for a quadrilateral element resistance blinder calculation is a field-proven ground element implemented in numerous relays [2] [5]. It is called a Type I resistance blinder in this paper.

In [5], the resistance calculation is performed using the following formula and the result is compared with the resistance reach setting R_{set} :

$$rAG = \frac{\text{Im} \left\{ VA \cdot (\angle ZL1 \cdot [IA + K0 \cdot IO])^* \right\}}{\text{Im} \left\{ \frac{3}{2} \cdot (I2 + IO) \cdot (\angle ZL1 \cdot [IA + K0 \cdot IO])^* \right\}} \leq R_{set} \quad (23)$$

For the resistance blinder type expressed by (23) and the elementary network shown in Fig. 1, it is possible to derive an exact mathematical expression providing the resistance coverage as a function of the resistance reach setting and the network parameters. The derivation of this expression is provided in Appendix B. The mathematical relation is:

$$Rf_{max} = R_{set} \cdot G1(C1, C0, K0, \psi) \quad (24)$$

with the G1 function equal to:

$$G1(C1, C0, K0, \psi) = \frac{\text{Im} \left\{ \left(\frac{3}{2} \right) \cdot \frac{(C1 + C0)}{2 \cdot C1 + C0 \cdot (1 + K0)} \cdot e^{-j\psi} \right\}}{\text{Im} \left\{ \frac{3}{[2 \cdot C1 + C0 \cdot (1 + K0)]} \cdot e^{-j\psi} \right\}} \quad (25)$$

Equation (24) allows us to determine the element resistance coverage as a function of the resistance setting, the line impedance positive-sequence angle ψ , the fault current distribution factors C1 and C0, and the zero-sequence compensating factor K0.

The only assumption made in the derivation of (25) is that the line loading is zero. If we make the further assumption of a homogeneous network, meaning the following angles are equal:

$$\angle C1 = \angle C0 = \angle K0 \quad (26)$$

an even simpler and still very accurate function G2 replaces G1 in (24):

$$G2(C1, C0) = \frac{\text{real}(C1 + C0)}{2} \quad (27)$$

In (27), the maximum value that the function G2 can take is 1. We can then infer that for the Type I blinder, the resistance coverage can never be more than the resistance reach setting R_{set} under any conditions.

1) Comparison Between the Network-Based and Equation-Based Approaches

Unlike the case of the mho ground element, we have been successful in deriving two equations that provide the resistance coverage as a function of the network parameters for the resistance blinder of Type I corresponding to (23).

In order to demonstrate the accuracy of (25) and (27), Fig. 14 shows three plots for the resistance coverage for the reference network of Fig. 3 using the two possible approaches: the approach based on the network resolution and the approach based on the solutions of (25) and (27). The three plots are almost identical. A very slight accuracy advantage should be given to (25), however.

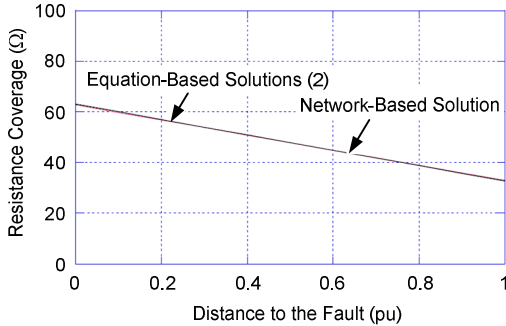


Fig. 14. Resistance coverage characteristic comparison between three solutions with the quadrilateral Type I blinder

2) Impact of Line Loading on the Ground Quadrilateral Resistance Coverage

In order to assess the effect of line loading on the resistance coverage, the angle of the right source has been set successively to 10, 0, and -10 degrees in Fig. 15.

Obviously, the line loading does not have any impact on the resistance coverage. This justifies the assumption made in the derivation of (25) and (27) that K_I could be set to 1. It also indicates that the resistance blinder calculation as provided by (23) is immune to any balanced load effect.

In view of this result, the remaining testing for the Type I resistance blinder will be done at no-load condition.

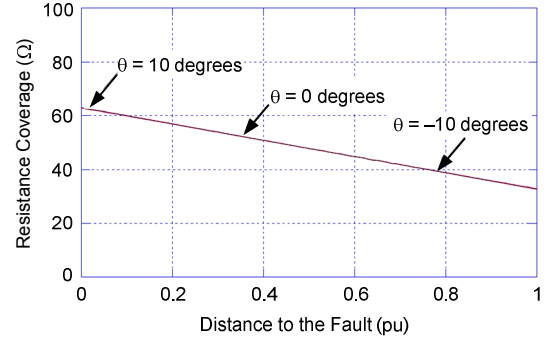


Fig. 15. Resistance coverage characteristics with three different load angles for the quadrilateral Type I blinder

3) Impact of the Right Source Sequence Impedances

When the right source impedances $ZR1$ and $ZR0$ become very large, both current distribution factors $C1$ and $C0$ become close to 1. Under this condition, the function G2 that determines the resistance coverage in (27) will tend toward unity.

$$\begin{aligned} ZR1 \ \& \ ZR0 \rightarrow \infty \Rightarrow C1 \ \& \ C0 \rightarrow 1 \\ C1 \ \& \ C0 \rightarrow 1 \Rightarrow G2(C1, C0) \rightarrow 1 \end{aligned} \quad (28)$$

Alternatively, when the right source sequence impedances tend toward 0 and the distance to the fault tends toward 1, the sequence current distribution factors will tend toward 0. Under this condition, the function G2 will tend toward zero.

$$\begin{aligned} (ZR1 \ \& \ ZR0 \rightarrow 0) \ \& \ (d \rightarrow 1) \Rightarrow C1 \ \& \ C0 \rightarrow 0 \\ (C1 \ \& \ C0 \rightarrow 0) \Rightarrow G2(C1, C0) \rightarrow 0 \end{aligned} \quad (29)$$

In Fig. 16, the right source sequence impedances ($ZR1$ and $ZR0$) have been successively multiplied by 0.1, 10, and 100.

Fig. 16 demonstrates what has been inferred mathematically: with large remote source impedance values, the resistance coverage becomes a quasi horizontal line, the level of which is equal to the resistance reach setting R_{set} . When the right source sequence impedances become smaller, the resistance coverage tends to zero when the fault is at the end of the line.

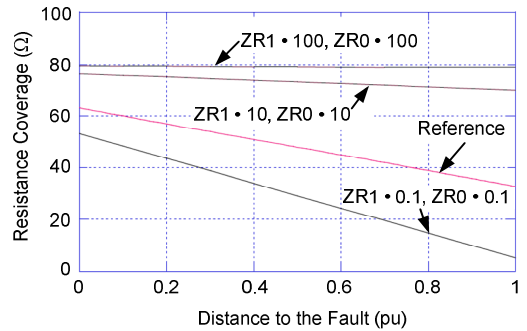


Fig. 16. Resistance coverage impact of the right source sequence impedances for the quadrilateral Type I blinder

4) Impact of the Left Source Sequence Impedances

Looking at the expression of $C1$ and $C0$ in (2) and (3) and at the expression of $G2$ in (27), we can infer that if we increase the value of the left source impedances, $C1$ and $C0$ will decrease because $ZS1$ and $ZS0$ are in the denominators of $C1$ and $C0$. When $C1$ and $C0$ in turn decrease, we have to expect the function $G2$ to decrease. Consequently, the resistance coverage will be smaller.

$$\begin{aligned} ZS1 \ \& \ ZS0 \uparrow \Rightarrow C1 \ \& \ C0 \downarrow \\ C1 \ \& \ C0 \downarrow \Rightarrow G2(C1, C0) \downarrow \end{aligned} \quad (30)$$

Alternatively, if we decrease the value of the left source impedances, $C1$ and $C0$ will increase. When $C1$ and $C0$ in turn increase, we have to expect the function $G2$ to increase. Consequently, the resistance coverage will be larger.

$$\begin{aligned} ZS1 \ \& \ ZS0 \downarrow \Rightarrow C1 \ \& \ C0 \uparrow \\ C1 \ \& \ C0 \uparrow \Rightarrow G2(C1, C0) \uparrow \end{aligned} \quad (31)$$

This has been verified in the simulation shown in Fig. 17, where $ZS1$ and $ZS0$ from the reference network have been multiplied successively by 0.1 and 10. The impact on the resistance coverage corresponds to what has been mathematically inferred by examination of the theoretical resistance coverage of (27).

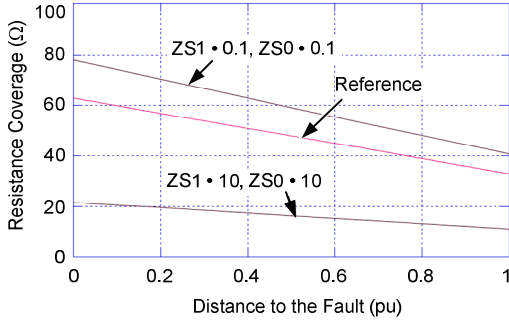


Fig. 17. Resistance coverage impact of the left source sequence impedances for the quadrilateral Type I blinder

5) Difference in Resistance Coverage Between the Relays at the Two Line Ends

In order to have the same resistance coverage for the two quadrilateral elements installed at each end of the line, we would need to have the same source impedances behind the two relays. This is something rarely achieved and would be difficult to verify due to the changing topology of the networks.

Fig. 18 shows the resistance coverage for the two quadrilateral elements installed at the two line ends of the reference network. The two elements are set to have the same resistance reach of 80 ohms. At a distance of 0.3 pu of the line length, for example, there is an obvious difference in resistance coverage between the two elements. Any resistive fault with a resistance value falling between the two characteristics will be detected by the left element but not by the right one. This situation could be corrected by increasing the resistance reach on the right element, but there is not much margin, given the maximum value of the reach setting as provided by (22).

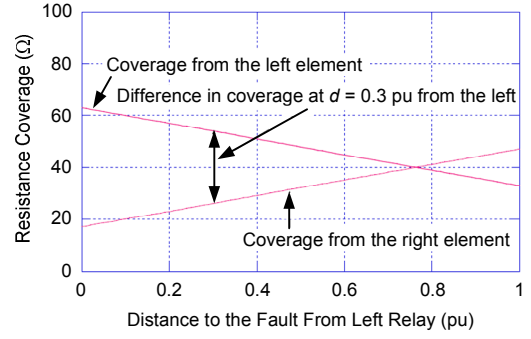


Fig. 18. Difference in resistance coverage between the left and right quadrilateral ground elements with the Type I blinder

6) Impact of the Open Breaker at the Line End

We assume again that the reference network transmission line is protected at both ends by quadrilateral elements. As discussed in the previous paragraphs, the possibility exists that the left-side element will assert first and open the left line breaker. With this new condition, the right-side element will see its resistance coverage change because the right source sequence impedances have now become infinite. Depending upon if the left-side breaker is open or not, the right-side quadrilateral element will switch between the two resistance coverage characteristics shown in Fig. 19.

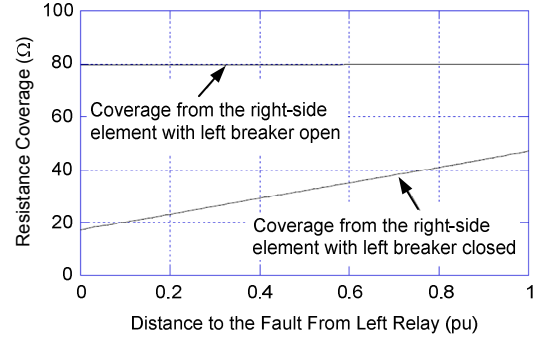


Fig. 19. Switch between two resistance coverage characteristics as a function of the remote-end breaker state for the quadrilateral Type I blinder

7) Impact of a Parallel Line on the Resistance Coverage

The last test on the current resistance blinder consists of adding a parallel line as shown in Fig. 2.

We can still use equations equivalent to (25) and (27), but the current distribution factors have to be switched to the expressions indicated in (7) and (8) for the parallel lines so that we get:

$$Rf_{\max} = R_{\text{set}} \cdot G1_p(C1_p, C0_p, K0, \psi) \quad (32)$$

$$\begin{aligned} G1_p(C1_p, C0_p, K0, \psi) = \\ \frac{\text{Im} \left\{ \left(\frac{3}{2} \right) \cdot \frac{(C1_p + C0_p)}{2C1_p + C0_p(1 + K0)} \cdot e^{-j\psi} \right\}}{\text{Im} \left\{ \frac{3}{[2C1_p + C0_p(1 + K0)]} \cdot e^{-j\psi} \right\}} \end{aligned} \quad (33)$$

$$G2_p(C1_p, C0_p) = \frac{\text{real}(C1_p + C0_p)}{2} \quad (34)$$

Again, the solution based on (33) or (34) provides an almost perfect match with the solution based on the network resolution.

With values for the impedance multiplier of 0.25, 1, and 4, Fig. 20 shows the impact of the parallel line on the resistance coverage in comparison with the reference model (network without the parallel line) in red. Obviously, the parallel line has an impact, particularly as the fault gets closer to the line end: the resistance coverage is reduced by more than a factor of 2 as n gets smaller (0.25 in the plot).

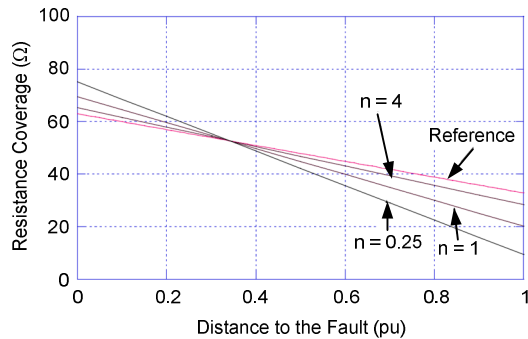


Fig. 20. Resistance coverage impact of parallel line with no coupling for the quadrilateral Type I blinder

D. Other Examples of Resistance Blinder Calculations

Other resistance blinder implementation principles have been used in relays. In [4], another approach was taken to perform the quadrilateral element resistance calculation and two resistance blinder principles were used. For the Phase A-to-ground impedance loop, the first resistance blinder, called Type II, is calculated using (35). It is polarized using negative-sequence (NS) current.

$$R_2 = \frac{\text{Im} \left[\text{VA} \cdot (I_2 \cdot e^{j\psi})^* \right]}{\text{Im} \left[(IA + K_0 \cdot I_0) \cdot (I_2 \cdot e^{j\psi})^* \right]} \leq R_{\text{set}} \quad (35)$$

For the second resistance blinder calculation, called Type III, (36) uses a combination of PS and NS current polarization.

$$R_2 = \frac{\text{Im} \left[\text{VA} \cdot ((I_1 + I_2) \cdot e^{j\psi})^* \right]}{\text{Im} \left[(IA + K_0 \cdot I_0) \cdot ((I_1 + I_2) \cdot e^{j\psi})^* \right]} \leq R_{\text{set}} \quad (36)$$

It is worth underscoring that the only difference between the blinder resistance for Types II and III is that the PS current has been added in the polarizing quantity of Type III. For a Phase A-to-ground fault, the only difference between the positive- and negative-sequence currents at the relay location is the load current. So it can be inferred that both blinders will have the same performance at no-load condition.

As indicated in Appendix C, making the assumption that there is no load and that the system is homogeneous, the following relation can be derived between the maximum

detectable fault resistance and the resistance setting for the Type II or III blinder:

$$R_{f_{\text{max}}} = \frac{R_{\text{set}}}{\text{real}(K_R)} \quad (37)$$

Type II or III resistance blinders are sensitive to the load. So, (37) can be used only at no load. Fig. 21 shows the resistance coverage for the network of Fig. 3 as seen from an element installed on the line left terminal using the two methods: the network-based solution and equation-based solution. The two solutions give results within 5 percent.

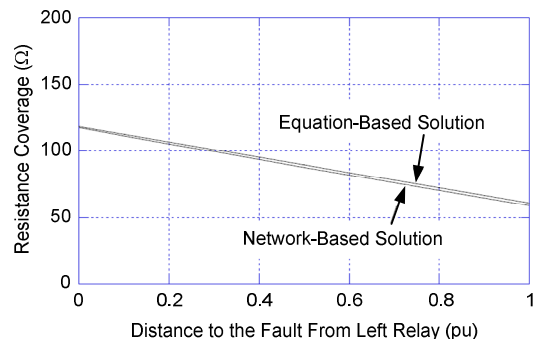


Fig. 21. Resistance coverage comparison between two solutions for the Type II or III blinder at zero load

An optimum resistance sensitivity, superior to the Type I blinder, is achieved in [4] by combining the two blinder calculation (Type II and Type III) logic outputs through an OR gate. The outcome of this combination, called Type II&III, has a resistance coverage that is generally (but not always) above the resistance reach setting.

In Fig. 22, the variation of the resistance coverage for the Type II&III blinder is shown for load angles of -10 , 0 , and 10 degrees. As already noted, the resistance can get well above the resistance reach setting.

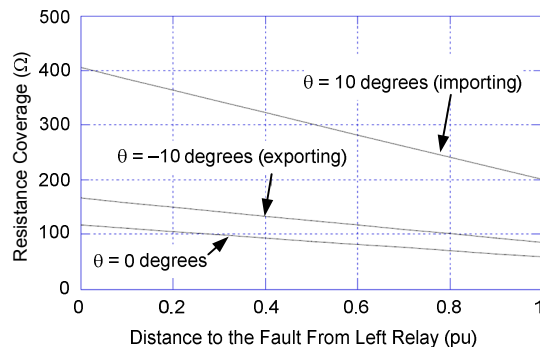


Fig. 22. Resistance coverage characteristics for Type II&III blinder at various load angles

Other than the line loading, the conclusions drawn for the Type I resistance blinder on the impact of the network parameters on the resistance coverage are applicable to the Type II&III resistance calculation. However, as noted previously, there are two major differences:

- The Type II&III blinder calculation could have resistance coverage higher than the resistance reach so

that it will be more sensitive than Type I, given that the resistance reach R_{set} is the same.

- The Type II&III blinder calculation is sensitive to the load.

As an example of the impact of the network parameters on the Type II&III resistance blinder combination, Fig. 23 shows the impact of the variation of the right source sequence impedances at zero load and with the same resistance setting as before (80 ohms). The plots in Fig. 23 are similar to the plots in Fig. 16, with the difference that the Type II&III blinder turns out to have more resistance coverage than Type I for the same resistance reach.

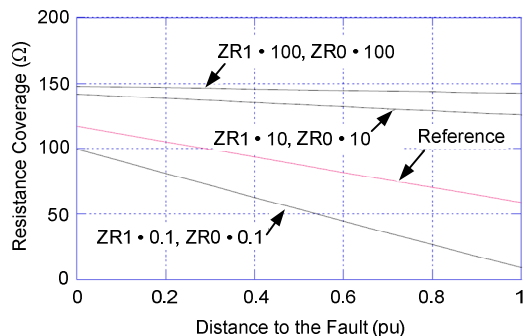


Fig. 23. Impact on the resistance coverage of the right source sequence impedances for the Type II&III blinder at zero load angle

V. CONCLUSION

The objective of this paper is to illustrate through a number of examples the impact of the network parameters on the resistance coverage of mho and quadrilateral ground elements.

Based on the testing discussed in this paper, the following observations can be made:

- Unlike some quadrilateral resistance blinder types, it is difficult with mho elements to derive an analytic expression that will provide a direct relation between the element resistance coverage and the network parameters.
- The resistance coverage of a mho element will always be zero at the element set distance reach.
- A very large resistance coverage for a ground mho element will take place with a radial system ($ZR1$ and $ZR0$ approaching infinity) and a long transmission line.
- The main difference between the mho and quadrilateral elements is that a resistance reach setting is introduced for the latter that allows superior resistance coverage.
- With mho elements, the resistance coverage is dependent upon the distance reach setting. With quadrilateral elements, it is completely independent.
- The Type I resistance blinder described in this paper has a maximum resistance coverage equal to the resistance reach setting. This blinder type is independent of load.
- The Type II&III resistance blinder described in this paper allows a resistance coverage that could be

greater than the resistance reach setting. The Type II&III resistance blinder therefore allows better sensitivity than Type I. However, resistance coverage will depend upon the load.

- With quadrilateral elements, regardless of the resistance blinder type, the maximum detected fault resistance occurs with faults close to the relay. The coverage is proportionally reduced as the distance to the fault increases. With radial lines, the resistance coverage becomes uniform and is practically not affected by the fault location.
- With a mho element, a long transmission line naturally calls for a better resistance coverage. With a quadrilateral element, a long transmission line allows setting a higher resistance reach so that the element retains its main advantage.

VI. APPENDIX A: RESOLUTION OF A SINGLE-PHASE A-TO-GROUND FAULT USING THE SEQUENCE NETWORKS

The superposition principle is used to resolve a single-Phase A-to-ground fault for the network of Fig. 1. The corresponding sequence network is shown in Fig. 24.

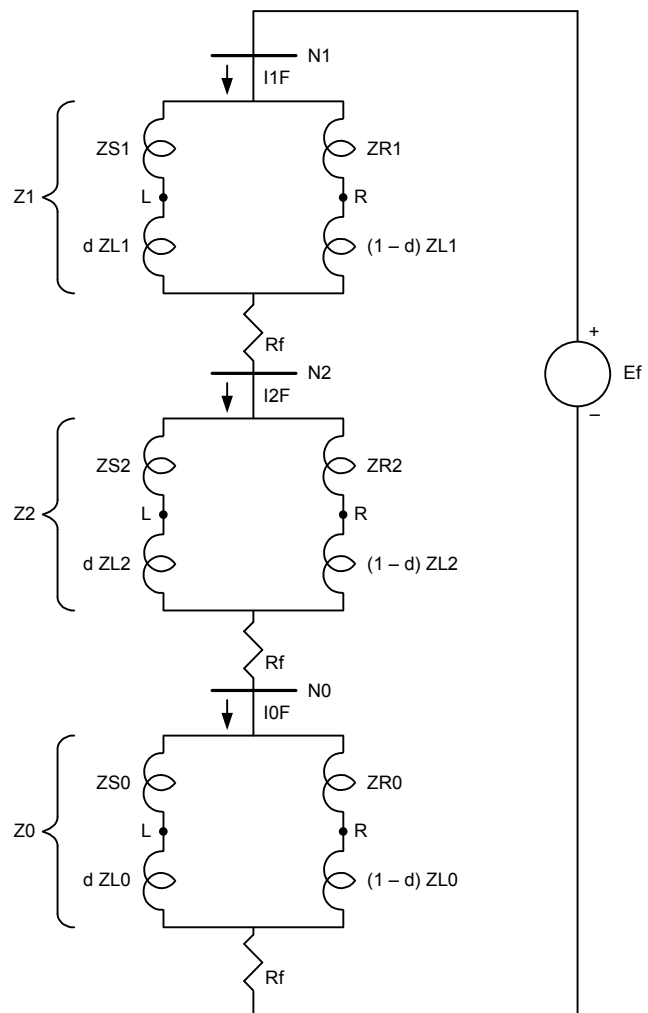


Fig. 24. Phase A-to-ground pure-fault sequence network

The load current is:

$$I_{LD} = \frac{(1 - e^{j\theta}) \cdot VA}{ZS1 + ZL1 + ZR1} \quad (38)$$

The voltage at the fault point before the fault is:

$$Ef = VA - I_{LD} \cdot (ZS1 + d \cdot ZL1) \quad (39)$$

The Phase A voltage at the relay before the fault is:

$$VA_{pre} = Ef + d \cdot ZL1 \cdot I_{LD} \quad (40)$$

The equivalent PS impedance is:

$$Z1 = Z2 = \frac{(ZS1 + d \cdot ZL1) \cdot (ZR1 + (1 - d) \cdot ZL1)}{ZS1 + ZL1 + ZR1} \quad (41)$$

The equivalent ZS impedance is:

$$Z0 = \frac{(ZS0 + d \cdot ZL0) \cdot (ZR0 + (1 - d) \cdot ZL0)}{ZS0 + ZL0 + ZR0} \quad (42)$$

The sequence currents at the fault point are:

$$I1F = I2F = I0F = \frac{Ef}{2 \cdot Z1 + Z0 + 3Rf} \quad (43)$$

The sequence currents at the relay are:

$$\begin{aligned} I1 &= I2 = C1 \cdot I1F \\ I0 &= C0 \cdot I0F \end{aligned} \quad (44)$$

The expressions of the PS and ZS current distribution factors $C1$ and $C0$ are provided by (2) and (3).

Applying the superposition principle, the Phase A current and voltage at the relay location are:

$$\begin{aligned} IA &= I_{LD} + 2 \cdot C1 \cdot I1F + C0 \cdot I0F \\ VA &= VA_{pre} - 2 \cdot C1 \cdot I1F \cdot ZS1 - C0 \cdot I0F \cdot ZS0 \end{aligned} \quad (45)$$

If we replace VA_{pre} in (45) by its expression in (40), we get:

$$VA = Ef + d \cdot ZL1 \cdot I_{LD} - 2 \cdot C1 \cdot I1F \cdot ZS1 - C0 \cdot I0F \cdot ZS0 \quad (46)$$

From the sequence network in Fig. 24, Ef can be otherwise expressed as:

$$\begin{aligned} Ef &= 2 \cdot C1 \cdot I1F \cdot (ZS1 + d \cdot ZL1) + \\ &C0 \cdot I0F \cdot (ZS0 + d \cdot ZL0) + 3 \cdot I1F \cdot Rf \end{aligned} \quad (47)$$

In (46), if we replace Ef with its value as expressed in (47), we get for VA :

$$\begin{aligned} VA &= d \cdot ZL1 \cdot I_{LD} + 2 \cdot C1 \cdot I1F \cdot \\ &d \cdot ZL1 + C0 \cdot I0F \cdot d \cdot ZL0 \end{aligned} \quad (48)$$

In (48), if we add up and subtract, to the right side of the equal sign, the same term $m \cdot ZL1 \cdot C0 \cdot I0F$, we get for VA :

$$\begin{aligned} VA &= d \cdot ZL1 \cdot \\ &(I_{LD} + 2 \cdot C1 \cdot I1F + C0 \cdot I0F + K0 \cdot C0 \cdot I0F) + 3 \cdot I1F \cdot Rf \end{aligned} \quad (49)$$

In this last expression, $K0$ is the zero-sequence compensation factor.

$$K0 = \frac{ZL0 - ZL1}{ZL1} \quad (50)$$

The compensated current to be supplied for the Phase A-to-ground fault impedance loop is:

$$IR = IA + K0 \cdot I0 \quad (51)$$

The ratio of VA as expressed in (49) over IR becomes simply:

$$\frac{VA}{IR} = d \cdot ZL1 \cdot \frac{3 \cdot I1F \cdot Rf}{IR} \quad (52)$$

In (51), if we replace IA by its value as provided by (45), we get for IR :

$$IR = I_{LD} + 2 \cdot C1 \cdot I1F + C0 \cdot I0F + K0 \cdot C0 \cdot I0F \quad (53)$$

From (53), we can extract $I1F$:

$$I1F = \frac{IR - I_{LD}}{2 \cdot C1 + C0 \cdot (1 + K0)} \quad (54)$$

If we replace $I1F$ in (52) by its expression in (54), we get:

$$\frac{VA}{IR} = d \cdot ZL1 \cdot \frac{3 \cdot (IR - I_{LD}) \cdot Rf}{IR \cdot (2 \cdot C1 + C0 \cdot (1 + K0))} \quad (55)$$

We define K_R as:

$$K_R = \frac{3}{2 \cdot C1 + C0 \cdot (1 + K0)} \quad (56)$$

We define K_I as:

$$K_I = \frac{IR}{IR - I_{LD}} \quad (57)$$

The apparent impedance for the Phase A-to-ground fault can finally be expressed as:

$$\frac{VA}{IR} = d \cdot ZL1 \cdot \frac{Rf \cdot K_R}{K_I} \quad (58)$$

Fig. 25 represents the sequence network for the case of the parallel lines of Fig. 2. The same equations as previously derived for the single-line case can be used by replacing the equivalent impedances $Z1$, $Z2$, and $Z0$ with $ZP1$, $ZP2$, and $ZP0$. The current distribution factors for the parallel lines can be determined by performing the proper delta-to-star impedance transformation in Fig. 25 and are provided in (7) and (8).

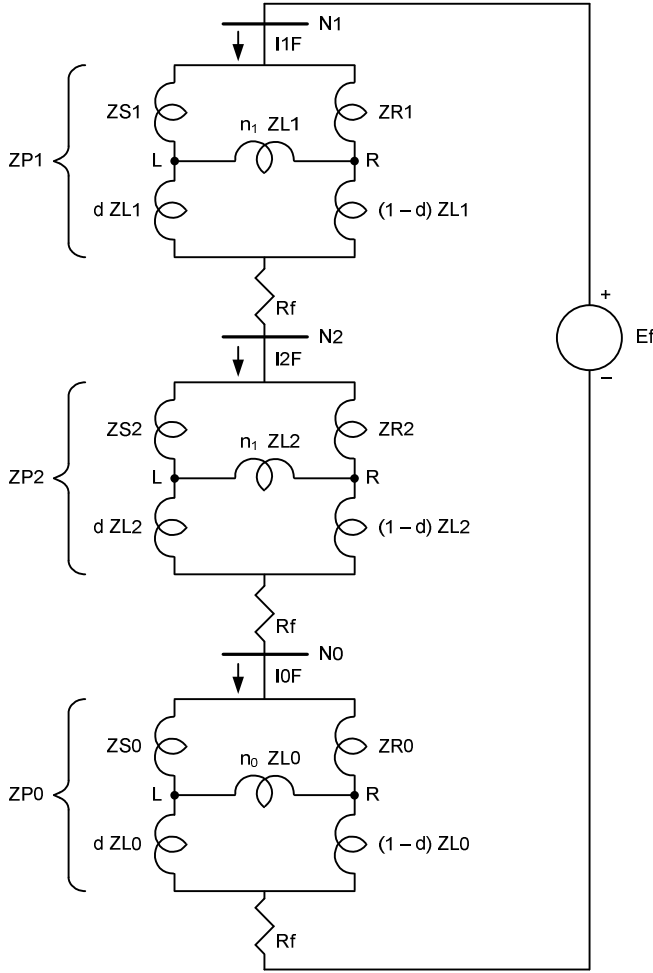


Fig. 25. Phase A-to-ground pure-fault sequence network with parallel line

VII. APPENDIX B: RELATION BETWEEN R_f AND R_{SET} FOR A TYPE I QUADRILATERAL ELEMENT RESISTANCE BLINDER

We have for the calculated resistance:

$$R_{AG} = \frac{\text{Im}\left\{V_A \cdot (\angle ZL1 \cdot [IA + K0 \cdot I0])^*\right\}}{\left\{\text{Im}\left(\frac{3}{2}\right) \cdot (I2 + I0) \cdot (\angle ZL1 \cdot [IA + K0 \cdot I0])^*\right\}} \quad (59)$$

Assume the angle of the line is expressed as:

$$\angle ZL1 = e^{j\psi} \quad (60)$$

Applying (1), V_A can be expressed as:

$$V_A = \left(d \cdot ZL1 + R_f \cdot \frac{K_R}{K_I}\right) \cdot (IA + K0 \cdot I0R) \quad (61)$$

Introducing the value of V_A in the numerator of (59):

$$\text{NUM} = \text{Im}\left\{\left(d \cdot ZL1 + R_f \cdot \frac{K_R}{K_I}\right) \cdot e^{-j\psi} \cdot |IA + K0 \cdot I0|^2\right\} \quad (62)$$

we have:

$$\text{Im}(d \cdot ZL1 \cdot e^{-j\psi}) = 0 \quad (63)$$

so that we end up finally with:

$$\text{NUM} = (IA + K0 \cdot I0)^2 \cdot \text{Im}\left\{R_f \cdot \frac{K_R}{K_I} \cdot e^{-j\psi}\right\} \quad (64)$$

The denominator can be expressed as:

$$\text{DEN} = \text{Im}\left\{\left(\frac{3}{2}\right) \cdot (C1 + C0) \cdot I1F \cdot (e^{j\psi} \cdot [IA + K0 \cdot I0])^*\right\} \quad (65)$$

so that the ratio can now be expressed as:

$$R_{AG} = \frac{|IA + K0 \cdot I0|^2 \cdot \text{Im}\left\{R_f \cdot \frac{K_R}{K_I} \cdot e^{-j\psi}\right\}}{\text{Im}\left\{\left(\frac{3}{2}\right) \cdot (C1 + C0) \cdot I1F \cdot (e^{j\psi} \cdot [IA + K0 \cdot I0])^*\right\}} \quad (66)$$

or:

$$R_{AG} = \frac{\text{Im}\left\{R_f \cdot \frac{K_R}{K_I} \cdot e^{-j\psi}\right\}}{\text{Im}\left\{\frac{3}{2} \cdot (C1 + C0) \cdot I1F \cdot e^{-j\psi} \cdot \frac{(IA + K0 \cdot I0)^*}{|IA + K0 \cdot I0|^2}\right\}} \quad (67)$$

or:

$$R_{AG} = \frac{\text{Im}\left\{R_f \cdot \frac{K_R}{K_I} \cdot e^{-j\psi}\right\}}{\text{Im}\left\{\frac{3}{2} \cdot \frac{(C1 + C0) \cdot I1F \cdot e^{-j\psi}}{(IA + K0 \cdot I0)}\right\}} \quad (68)$$

Looking at the sequence network of Fig. 24 for a Phase A-to-ground fault, we have for the compensated current:

$$IA + K0 \cdot I0 = I_{LD} + (2C1 + C0) \cdot I1F + K0 \cdot C0 \cdot I1F \quad (69)$$

so that we have:

$$R_{AG} = \frac{\text{Im}\left\{R_f \cdot \frac{K_R}{K_I} \cdot e^{-j\psi}\right\}}{\text{Im}\left\{\left(\frac{3}{2}\right) \cdot \frac{(C1 + C0) I1F}{[2C1 + C0(1 + K0)] I1F + I_{LD}} \cdot e^{-j\psi}\right\}} \leq R_{set} \quad (70)$$

If we assume that there is no load ($I_{LD} = 0$ and $K_I = 1$), we end up finally with:

$$R_{AG} = \frac{\text{Im}\left\{R_f \cdot K_R \cdot e^{-j\psi}\right\}}{\text{Im}\left\{\left(\frac{3}{2}\right) \cdot \frac{(C1 + C0)}{2C1 + C0(1 + K0)} \cdot e^{-j\psi}\right\}} \leq R_{set} \quad (71)$$

Equation (71) can be otherwise expressed as:

$$R_f \leq \frac{R_{set} \cdot \text{Im}\left\{\left(\frac{3}{2}\right) \cdot \frac{(C1 + C0)}{2C1 + C0(1 + K0)} \cdot e^{-j\psi}\right\}}{\text{Im}\left\{K_R \cdot e^{-j\psi}\right\}} \quad (72)$$

The element resistance coverage is obtained by switching the inequality sign to the equality sign:

$$R_{f_{\max}} = \frac{R_{\text{set}} \cdot \text{Im} \left\{ \left(\frac{3}{2} \right) \cdot \frac{(C1 + C0)}{2C1 + C0(1 + K0)} \cdot e^{-j\psi} \right\}}{\text{Im} \{ K_R \cdot e^{-j\psi} \}} \quad (73)$$

VIII. APPENDIX C: RELATION BETWEEN R_f AND R_{SET} FOR TYPES II AND III QUADRILATERAL ELEMENT RESISTANCE BLINDERS

For the Type II quadrilateral, the resistance calculation uses the negative-sequence current polarization and is provided by the following:

$$R_2 = \frac{\text{Im} \left[VA \cdot (I_2 \cdot e^{j\psi})^* \right]}{\text{Im} \left[(IA + k0 \cdot I0) \cdot (I_2 \cdot e^{j\psi})^* \right]} < R_{\text{set}} \quad (74)$$

As in Appendix B, we assume for the line angle:

$$\angle ZL1 = e^{j\psi} \quad (75)$$

Introducing the expression of VA as provided by (61), we get for the numerator of (74):

$$\text{NUM} = \text{Im} \left[\left(d \cdot ZL1 + \frac{R_f}{K_I} K_R \right) \cdot (IA + K0 \cdot I0) \cdot I_2^* \cdot e^{-j\psi} \right] \quad (76)$$

At no load ($K_I = 1$) and if the system is homogeneous, the next equality applies:

$$\text{Im} \left[(IA + K0 \cdot I0) \cdot I_2^* \right] = 0 \quad (77)$$

so that we are left for (74) with:

$$R_2 = \frac{\text{Im} (R_f \cdot K_R \cdot e^{-j\psi})}{\text{Im} (e^{-j\psi})} < R_{\text{set}} \quad (78)$$

Equation (78) can be otherwise expressed as:

$$R_f \leq \frac{R_{\text{set}}}{\text{real}(K_R)} \quad (79)$$

It has already been underscored that at no-load condition, both blinder Types II and III have the same performance. Because (79) is only valid at no-load condition, we can say that it is applicable to both blinder Types II and III.

IX. REFERENCES

- [1] IEEE Standard C37.114, IEEE Guide for Determining Fault Location on AC Transmission and Distribution Lines.
- [2] E. O. Schweitzer, III and J. Roberts, "Distance Relay Element Design," proceedings of the 46th Annual Conference for Protective Relay Engineers, College Station, TX, April 1993.
- [3] E. O. Schweitzer, III, K. Behrendt, and T. Lee, "Digital Communications for Power System Protection: Security, Availability, and Speed," proceedings of the 25th Annual Western Protective Relay Conference, Spokane, WA, October 1998.
- [4] F. Calero, A. Guzmán, and G. Benmouyal, "Adaptive Phase and Ground Quadrilateral Distance Elements," proceedings of the 36th Annual Western Protective Relay Conference, Spokane, WA, October 2009.

- [5] J. Mooney and J. Peer, "Application Guidelines for Ground Fault Protection," proceedings of the 24th Annual Western Protective Relay Conference, Spokane, WA, October 1997.

X. FURTHER READING

J. Roberts, A. Guzmán, and E. O. Schweitzer, III, "Z = V/I Does Not Make a Distance Relay," proceedings of the 20th Annual Western Protective Relay Conference, Spokane, WA, October 1993.

E. O. Schweitzer, III and J. J. Kumm, "Statistical Comparison and Evaluation of Pilot Protection Schemes," proceedings of the 23rd Annual Western Protective Relay Conference, Spokane, WA, October 1996.

S. Ward, "Comparison of Quadrilateral and Mho Distance Characteristic," proceedings of the 26th Annual Western Protective Relay Conference, Spokane, WA, October 1999.

V. Terzija and H. Koglin, "New Approach to Arc Resistance Calculation," IEEE PES Winter Meeting, Vol. 2, 2001.

G. Swift, D. Fedirchuk, and T. Ernst, "Arcing Fault 'Resistance' (It Isn't)," proceedings of the 6th Annual Georgia Tech Fault and Disturbance Analysis Conference, Atlanta, GA, May 2003.

J. Holbach, V. Vadlamani, and Y. Lu, "Issues and Solutions in Setting a Quadrilateral Distance Characteristic," proceedings of the 61st Annual Conference for Protective Relay Engineers, College Station, TX, April 2008.

XI. BIOGRAPHIES

Gabriel Benmouyal, P.E. received his B.A.Sc. in electrical engineering and his M.A.Sc. in control engineering from Ecole Polytechnique, Université de Montréal, Canada in 1968 and 1970, respectively. In 1969, he joined Hydro-Québec as an instrumentation and control specialist. He worked on different projects in the field of substation control systems and dispatching centers. In 1978, he joined IREQ, where his main field of activity was the application of microprocessors and digital techniques for substation and generating station control and protection systems. In 1997, he joined Schweitzer Engineering Laboratories, Inc. in the position of principal research engineer. He is a registered professional engineer in the Province of Québec, is an IEEE senior member, and has served on the Power System Relaying Committee since May 1989. He holds more than six patents and is the author or coauthor of several papers in the field of signal processing and power network protection and control.

Armando Guzmán received his BSEE with honors from Guadalajara Autonomous University (UAG), Mexico. He received a diploma in fiber-optics engineering from Monterrey Institute of Technology and Advanced Studies (ITESM), Mexico, and his MSEE and MECE from the University of Idaho, USA. He lectured at UAG and the University of Idaho in power system protection and power system stability. Since 1993, Armando has been with Schweitzer Engineering Laboratories, Inc. in Pullman, Washington, where he is a fellow research engineer. He holds several patents in power system protection and metering. He is a senior member of IEEE.

Rishabh Jain is pursuing his master's degree in electrical engineering at the University of Idaho. In 2011, he completed his bachelor's degree in electrical engineering from Indian School of Mines University, Dhanbad, India. Previously, he worked for National Mineral Development Corporation Limited as an operations engineer. He works as a research engineering intern in the protection systems research group at Schweitzer Engineering Laboratories, Inc. His research interests are in grid integration of distributed resources, micro-scale renewables, energy optimization, and electricity market design.